Taspase1-dependent TFIIA cleavage coordinates head morphogenesis by limiting *Cdkn2a* locus transcription

Shugaku Takeda,[1] Satoru Sasagawa,[2] Toshinao Oyama,[1] Adam C. Searleman,[3] Todd D. Westergard,[3] Emily H. Cheng,[1,4,5] and James J. Hsieh[1,6,7]

[1]Human Oncology and Pathogenesis Program, Memorial Sloan-Kettering Cancer Center, New York, New York, USA. [2]Department of Biology, Osaka Medical Center for Cancer and Cardiovascular Diseases, Osaka, Japan. [3]Department of Medicine, Washington University School of Medicine, St. Louis, Missouri, USA. [4]Department of Pathology, Memorial Sloan-Kettering Cancer Center, New York, New York, USA. [5]Department of Pathology, Weill Medical College of Cornell University, New York, New York, USA. [6]Department of Medicine, Memorial Sloan-Kettering Cancer Center, New York, New York, USA. [7]Department of Medicine, Weill Medical College of Cornell University, New York, New York, USA.

Head morphogenesis requires complex signal relays to enable precisely coordinated proliferation, migration, and patterning. Here, we demonstrate that, during mouse head formation, taspase1-mediated (TASP1-mediated) cleavage of the general transcription factor TFIIA ensures proper coordination of rapid cell proliferation and morphogenesis by maintaining limited transcription of the negative cell cycle regulators *p16Ink4a* and *p19Arf* from the *Cdkn2a* locus. In mice, loss of TASP1 function led to catastrophic craniofacial malformations that were associated with inadequate cell proliferation. Compound deficiency of *Cdkn2a*, especially *p16Ink4a* deficiency, markedly reduced the craniofacial anomalies of TASP1-deficent mice. Furthermore, evaluation of mice expressing noncleavable TASP1 targets revealed that TFIIA is the principal TASP1 substrate that orchestrates craniofacial morphogenesis. ChIP analyses determined that noncleaved TFIIA accumulates at the *p16Ink4a* and *p19Arf* promoters to drive transcription of these negative regulators. In summary, our study elucidates a regulatory circuit comprising proteolysis, transcription, and proliferation that is pivotal for construction of the mammalian head.

Introduction

Morphogenesis of mammalian heads is a complex process coordinating differential cell proliferation, death, migration, and patterning in all germ layers. Craniofacial malformations in humans are major congenital disorders and a primary cause of infant mortality (1, 2). More than 700 distinct human craniofacial anomalies have been described, including cleft lip, cleft palate, Treacher Collins syndrome, and holoprosencephaly. However, our knowledge of the genetic and environmental factors causing these anomalies is as yet very limited; this has hindered the development of effective treatments and preventative care for most of these anomalies.

Vertebrate animal models have been effective tools for understanding the conserved molecular processes governing head morphogenesis. In mammals, the prospective brain (anterior neuroectoderm) is induced by the anterior visceral endoderm and subsequently transforms into the anterior neural plate. Transcription factors, such as OTX2, LIM1, SSDP1, and HEX, and signaling pathways, such as WNT and BMP, define the complex network involved in this anterior specification (3–8). Upon neurulation, the anterior neural plate forms a neural tube that subdivides into 3 vesicles: the prosencephalon (forebrain), mesencephalon (midbrain), and rhombencephalon (hindbrain) (9). When neural progenitor cells increase in population, the brain vesicles experience robust size expansion, with a cell cycle time of 7 hours in the prosencephalon and 8.5 hours in more caudal regions (10, 11). Impor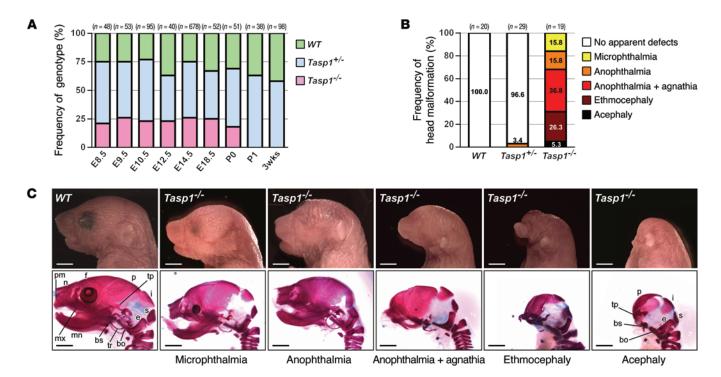tantly, cell proliferation is tightly controlled during brain expansion (12, 13). Poor cell cycle regulation is associated with a variety of head malformations (1, 2). However, the specific cell cycle factors involved in craniofacial morphogenesis have remained obscure. Their discovery is challenging, likely due to functional redundancy, such that the null alleles of cyclins, cyclin-dependent kinases (CDKs), and CDK inhibitors (CDKIs) do not incur overt craniofacial defects (14, 15).

Site-specific proteolysis regulates a variety of physiological and cellular processes, including the activation of caspases for cell death execution and the cleavage of the Notch intracellular domain for cell fate determination (16). Taspase1 (TASP1; threonine aspartase) is a 50-kDa endopeptidase of a family of hydrolases possessing an asparaginase 2 homology domain (17, 18). Our initial genetic study of *taspase1*-null (*Tasp1^{-/-}*) mice uncovered a critical role for TASP1 in cell cycle control (19). *Tasp1^{-/-}* mice exhibited decreased overall body size; *Tasp1^{-/-}* mouse embryonic fibroblasts (MEFs) exhibited impaired cell cycle progression, with upregulation of CDKIs *p16Ink4a*, *p21Cip1*, and *p27Kip1* and downregulation of *Ccne1*, *Ccna2*, and *Ccnb* (19). Bona fide TASP1 substrates with conserved IXQL(V)D/G cleavage site motifs include a ubiquitously expressed general transcription factor TFIIα-β, a testis-enriched general transcription factor ALFα-β (TFIIA-like factor), histone methyltransferases MLL1 (also known as MLL) and MLL2 (also known as MLL4), and *Drosophila* HCF (19–22). We discovered that TASP1-mediated proteolysis activates the full histone methyltransferase activities of MLL1 and MLL2, which in turn target cyclin gene promoters via E2F transcription factors (19, 23). On the other hand, it remained unclear how TASP1 mediates the transcriptional regulation of CDKIs.

Figure 1. Craniofacial malformations observed in *Tasp1⁻/⁻* mice. (A) Frequencies of live WT, *Tasp1⁺/⁻*, and *Tasp1⁻/⁻* animals observed at the indicated developmental stages. The expected genotype percentages from this intercross are 25%, 50%, and 25% for WT, *Tasp1⁺/⁻*, and *Tasp1⁻/⁻*, respectively. The reduction of the *Tasp1⁻/⁻* frequency between E18.5 and P1 indicates perinatal lethality. **(B)** Frequencies of the head malformations in WT, *Tasp1⁺/⁻*, and *Tasp1⁻/⁻* P0 pups. *Tasp1*-deficient animals displayed a range of head and face deformities. **(C)** Images on the top row are representative *Tasp1⁻/⁻* pups exhibiting smaller eyes (microphthalmia), absence of eyes (anophthalmia), lack of jaw (agnathia), and rod-like nose (ethmocephaly) as well as complete absence of craniofacial structures anterior to the ears (acephaly). Scale bar: 2.0 mm. Images on the bottom row show malformation of skull derivatives. Skull structures are identified where indicated. bo, basioccipital bone; bs, basisphenoid; e, exoccipital bone; f, frontal bone; i, interparietal bone; mn, mandible; mx, maxilla; n, nasal bone; p, parietal bone; pm, premaxilla; s, supraoccipital bone; tp, temporal bone; tr, tympanic ring.

The critical step of mRNA transcription is the recruitment and assembly of a transcription preinitiation complex, which consists of RNA polymerase II and general transcription factors (TFIIA, TFIIB, TFIID, TFIIE, TFIIF, and TFIIH) (24–26). TFIIA enhances transcription by stabilizing the binding of TATA-binding protein (TBP) at the promoter DNA and by counteracting the inhibitory effects of negative cofactors, like NC2/Dr1 and TAF1 (27–29). In higher eukaryotes, TFIIA exists as a heterotrimer composed of 3 subunits: α, β, and γ. TFIIAα-β is translated as a single polypeptide and site specifically proteolyzed by TASP1 into α and β subunits (30). Biochemical studies revealed that cleavage of TFIIAα-β increases susceptibility to proteasome-mediated degradation but does not affect TFIIA's ability to enhance transcription in vitro (31). Importantly, cleaved and noncleaved TFIIAα-β are equally capable of interacting with the TFIIAγ subunit and with TBP. Recently, we generated a knockin mouse expressing a noncleavable mutant form of TFIIAα-β and discovered that TFIIA proteolysis promotes TFIIA-mediated targeting of TBP-related factor 2 (TRF2) at the spermiogenic gene loci (*Tnp* and *Prm*) in a testis-specific manner (32). Consequently, TASP1 noncleavable TFIIAα-β knockin (*Tfiia^nc/nc*) mice exhibit male sterility (32).

Here, we report that the TASP1-mediated proteolysis of TFIIAα-β actively represses the transcription of negative cell cycle regulators *p16Ink4a* and *p19Arf*, transcribed from the *Cdkn2a* locus, to enable proper mammalian head development. TASP1 deficiency in mice leads to fatal craniofacial malformations and impaired telence-

phalic cell proliferation. Noncleaved TFIIAα-β is more stable and accumulates at *p16Ink4a* and *p19Arf* promoters. Excessive *p16Ink4a* and *p19Arf* transcription and aberrant craniofacial formation result when there is no TASP1 or TASP1 is unable to proteolyze TFIIAα-β. Together, our genetic and biochemical studies establish what we believe to be a novel essential pathway for mammalian head morphogenesis in which transcription of cell cycle regulators (*p16Ink4a* and *p19Arf*) is modulated via posttranslational site-specific proteolysis of a general transcription factor, TFIIAα-β.

Results

TASP1 deficiency leads to craniofacial malformations. Our initial study of TASP1-deficient mice on a mixed 129SvJ/C57BL/6 (N2) genetic background revealed that *Tasp1⁻/⁻* pups typically die on P1, without a visible milk spot (19). Skeletal and histological analysis revealed that newborn (P0) *Tasp1⁻/⁻* pups had a shortened skull and a distorted tongue (Supplemental Figure 1, A and B; supplemental material available online with this article; doi:10.1172/JCI77075DS1), which suggests that their demise resulted from suckling defects. Studies in mice deficient for *Otx2* or *Lim1*, two master transcription factors for mammalian head morphogenesis, have shown that the murine C57BL/6 genetic background is associated with greater susceptibility to head malformation (33, 34). Hence, our original line of *Tasp1⁺/⁻* mice was backcrossed to C57BL/6 mice. Interestingly, backcrossing beyond 6 generations
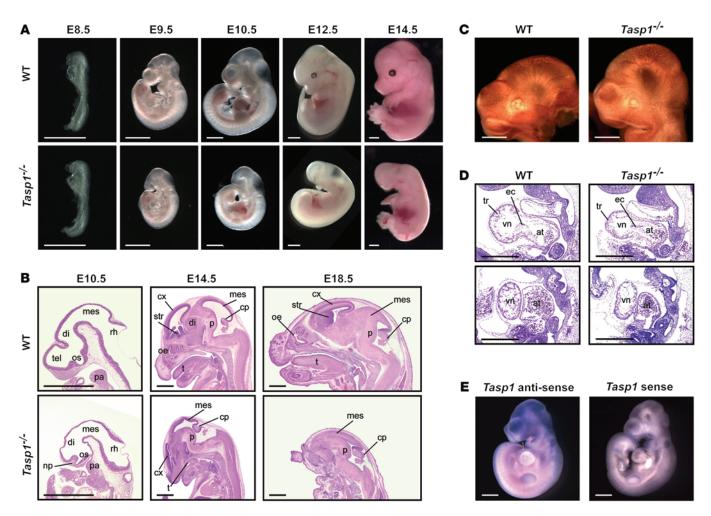
Figure 2. Disruption of brain architecture in *Tasp1*⁻/⁻ embryos. (**A**) Lateral views of representative WT and *Tasp1*⁻/⁻ embryos at different developmental stages (E8.5–E14.5). *Tasp1*⁻/⁻ embryos at E9.5 and older show truncations of head structures (93.8% at E9.5, *n* = 16; 93.0% at E10.5, *n* = 41; 100% at E12.5, *n* = 12; 94.3% at E14.5, *n* = 175). Scale bar: 1.0 mm. (**B**) Hematoxylin and eosin–stained sagittal sections of WT and *Tasp1*⁻/⁻ heads at the indicated developmental stages. Skull structures are identified where indicated. Note the hypoplasia of prosencephalic derivatives in *Tasp1*⁻/⁻ embryos. cp, choroid plexus; cx, cerebral cortex; di, diencephalon; mes, mesencephalon; np, nasal process; oe, olfactory epithelium; os, optic stalk; p, pons; pa, first pharyngeal arch; rh, rhombencephalon; str, striatum; t, tongue; tel, telencephalon. Scale bar: 1.0 mm. (**C**) Whole-mount anti-CD31 IHC of E10.5 WT and *Tasp1*⁻/⁻ embryos showing spreading of cranial vessels throughout entire heads. At least 3 embryos were tested for each group. Scale bar: 0.5 mm. (**D**) Hematoxylin and eosin–stained sagittal sections of WT and *Tasp1*⁻/⁻ E10.5 embryos. *Tasp1*⁻/⁻ hearts are smaller but exhibit normal development. at, atrium; ec, endocardial cushion; tr, myocardial trabeculae; vn, ventricle. At least 3 embryos were tested for each group. Scale bar: 0.5 mm. (**E**) Whole-mount in situ hybridization with *Tasp1* antisense and sense (negative control) probes on E10.5 WT embryos. *Tasp1* mRNA was detected at brain ventricles, pharyngeal arches, and limb buds. At least 3 embryos were tested for each probe. Scale bar: 1.0 mm.

resulted in marked infertility of *Tasp1*⁺/⁻ males (32). *Tasp1*⁻/⁻ mice were born from *Tasp1*⁺/⁻ (N6) intercrosses at near the expected Mendelian ratio, but all died within the first day after birth (Figure 1A). Strikingly, all these C57BL/6 background–enriched *Tasp1*⁻/⁻ mice displayed arrays of craniofacial malformations, ranging from smaller eyes (microphthalmia), absence of eyes (anophthalmia), absence of lower jaw (agnathia), and rod-like nose (ethmocephaly) to complete absence of head structures anterior to the ears (acephaly) (Figure 1, B and C). In acephalic *Tasp1*⁻/⁻ pups, the facial bones rostral to the parietal bones were missing or severely deformed, whereas caudal bones, such as the interparietal and suboccipital bones, were present (Figure 1C). On the other hand, we did not observe overt craniofacial defects in the 129SvJ background–enriched *Tasp1*⁻/⁻ pups from intercrosses of *Tasp1*⁺/⁻ mice that had been backcrossed to the 129SvJ strain for 6 generations.

Prenatal examinations of embryos demonstrated that more than 90% of *Tasp1*⁻/⁻ embryos at developmental stages E9.5 to E14.5 displayed major craniofacial defects, whereas E8.5 *Tasp1*⁻/⁻ embryos were indistinguishable from their WT littermates (Figure 2A and Supplemental Figure 2A). The prosencephalons, nasal processes, and first pharyngeal arches of *Tasp1*⁻/⁻ embryos (E9.5–E10.5) were hypoplastic or absent (Figure 2, A and B). E14.5–E18.5 *Tasp1*⁻/⁻ embryos exhibited severe underdevelopment or complete absence of the cerebral cortex and striatum as well as absence of the tongue and lower jaw (Figure 2, A and B). Additionally, most *Tasp1*⁻/⁻ embryos at developmental stages later than E9.5 displayed smaller trunk sizes compared with those of their WT littermates (Figure 2A). Interestingly, this marked reduction in body length distinguishes *Tasp1*-deficient animals from mice lacking different head organizer genes, like *Otx2-*, *Lim1-*, *Ssdp1-*, *Hex-*, *Hesx1-*,
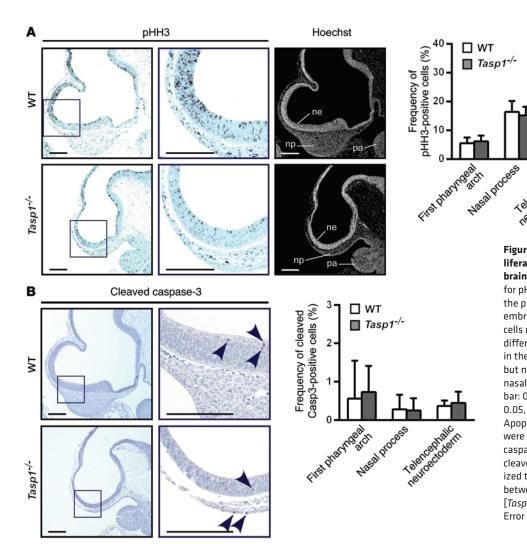
Figure 3. *Tasp1* loss results in reduced proliferation in the *Tasp1⁻/⁻* developing forebrain. (**A**) Immunohistochemical staining for pHH3 reveals reduced mitotic growth in the prosencephalic region of E10.5 *Tasp1⁻/⁻* embryos. The percentage of pHH3-positive cells normalized to Hoechst-positive cells differed between WT and *Tasp1⁻/⁻* embryos in the telencephalic neuroectoderm (ne) but not in the first pharyngeal arch or the nasal process ($n = 3$ throughout). Scale bar: 0.2 mm. Error bars represent SD. *$P < 0.05$, unpaired 2-tailed Student's t test. (**B**) Apoptotic cells in the E10.5 prosencephalon were observed by IHC detection of cleaved caspase-3 (arrowheads). The percentage of cleaved caspase-3–positive cells normalized to Hoechst-positive cells did not differ between WT and *Tasp1⁻/⁻* embryos ($n = 6$ [*Tasp1⁻/⁻*]; $n = 5$ [WT]). Scale bar: 0.2 mm. Error bars represent SD.

and *Dkk1*-deficient animals (5–7, 34–37). *Tasp1*-deficient animals have cranial morphogenetic defects, with normal or only slightly smaller body dimensions. Defects in the cardiovascular system can impede expansion of embryonic tissues by limiting distribution of nutrient and oxygen. However, this is unlikely the cause for craniofacial defects in *Tasp1⁻/⁻* embryos, because they exhibited normal development of cranial blood vessels (Figure 2C) and the heart (primitive ventricle, atrium, endocardial cushion, and myocardial trabeculae) (Figure 2D). Furthermore, whole-mount in situ hybridization of E10.5 embryos indicated prominent expression of TASP1 in the brain ventricles, pharyngeal arches, and limb buds (Figure 2E). This distinct pattern of TASP1 expression is consistent with the major phenotypes of *Tasp1⁻/⁻* embryos seen in head and pharyngeal arches.

The telencephalons of Tasp1⁻/⁻ animals exhibit impaired cell proliferation. Our prior studies using MEFs identified cyclin genes, genes encoding CDKIs, and *Hox* genes as the key downstream transcriptional effectors regulated by TASP1 through site-specific proteolysis of nuclear factors (19). It is unlikely that the *Hox* code has any influence on forebrain development, as the cephalic expression boundary of *Hox* genes is at the rhombomere (38). Thus, we focused on investigating whether a disruption of pro-

liferation accounts for the abnormal development of the *Tasp1⁻/⁻* prosencephalon. In comparison with that in WT embryos, E10.5 *Tasp1⁻/⁻* embryos showed reduced thickness of the telencephalic neuroectoderm, which was composed of 5 to 8 layers of neural progenitor cells, rather than the normal 6 to 10 layers (Figure 3A). Moreover, significantly fewer mitotically active cells were detected in *Tasp1⁻/⁻* prosencephalons by phospho–histone H3 (pHH3) staining than in WT prosencephalons (Figure 3A). The pHH3-positive WT cells were ordinarily widely distributed, whereas the few *Tasp1⁻/⁻* proliferating cells were restricted to the ventricular side (Figure 3A). On the other hand, comparable proliferation was detected in *Tasp1⁻/⁻* and WT first pharyngeal arches and nasal compartments (Figure 3A). Of note, *Tasp1⁻/⁻* and WT E10.5 prosencephalons showed no difference in apoptosis (Figure 3B).

Cdkn2a deficiency rescues the craniofacial and body size anomalies of Tasp1⁻/⁻ embryos. To elucidate how TASP1 organizes head morphogenesis, we performed comparative microarray analyses on prosencephalons and mesencephalons from E10.5 *Tasp1⁻/⁻* and WT embryos. Gene Ontology analysis revealed that the genes that were associated with "cell proliferation" and "metabolic process" are overrepresented among the genes differentially expressed between *Tasp1⁻/⁻* and WT embryo heads (Figure
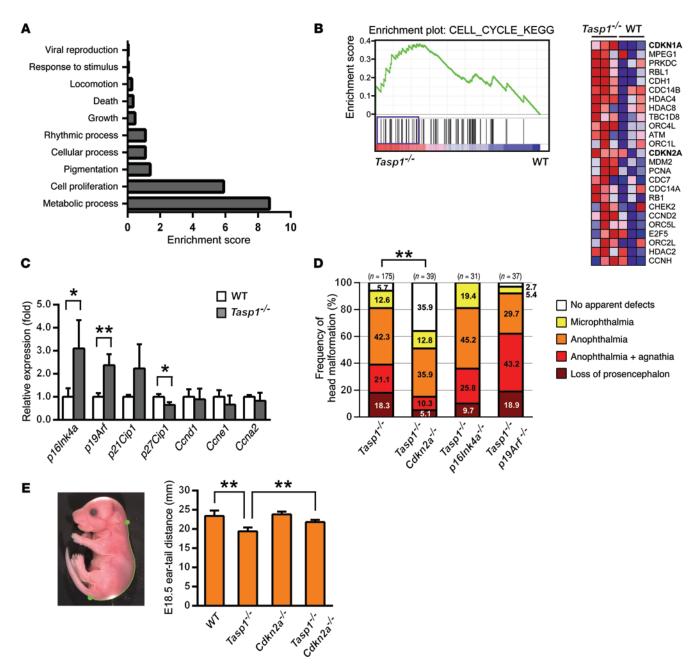
Figure 4. Craniofacial and body size anomalies of *Tasp1*^{−/−} embryos are rescued by *Cdkn2a* deficiency. (**A**) RNA harvested from E10.5 WT and *Tasp1*^{−/−} heads was subjected to microarray. Gene Ontology analysis shows functional categories of differentially expressed genes in the order of the enrichment score. (**B**) GSEA of expression signals from WT and *Tasp1*^{−/−} samples. Enrichment plot of the "CELL_CYCLE_KEGG" gene set, indicating enrichment of cell cycle–associated genes among significantly upregulated mRNAs in *Tasp1*^{−/−} heads ($P < 0.01$, normalized enrichment scores = 1.57). Genes showing core enrichment (indicated by inclusion in the purple bar under the enrichment plot) are listed by relative expression (red, high; blue, low). (**C**) Increased *p16Ink4a* and *p19Arf* mRNA levels were detected in E10.5 *Tasp1*^{−/−} embryonic heads by quantitative RT-PCR ($n = 3$ throughout). Error bars represent SD. *$P < 0.05$, **$P < 0.01$, unpaired 2-tailed Student's *t* test. (**D**) Frequencies of the otocephalic phenotypes in E14.5 embryos of the indicated genotypes. Note that *Cdkn2a* deficiency significantly rescued *Tasp1*^{−/−} craniofacial malformations. **$P < 0.01$, Fisher's exact test. (**E**) Body sizes of E18.5 embryos of the indicated genotypes. The distance from the ears to the base of tail was measured using ImageJ analysis. Note that *Cdkn2a* deficiency significantly rescued the reduced body sizes of *Tasp1*^{−/−} embryos ($n = 4$ throughout). Error bars represent SD. **$P < 0.01$, unpaired 2-tailed Student's *t* test.

4A). Gene set enrichment analysis (GSEA) of the Molecular Signature Database (C2 canonical pathways) indicates that 4 of the 20 gene sets with the highest normalized enrichment scores are associated with cell proliferation (Figure 4B and Supplemental Table 1). These 4 gene sets commonly contain the negative cell cycle regulators *p21Cip1* (also known as *Cdkn1a*) and *Cdkn2a*

(Figure 4B). On the other hand, none of the gene sets associated with head development was overrepresented in GSEA. The *Cdkn2a* locus encodes 2 distinct proteins from alternative reading frames: p16Ink4a, which is a CDKI, and p19Arf, which promotes p53-dependent apoptosis and cell cycle arrest (39). Quantitative RT-PCR analyses demonstrated that the mRNA levels of
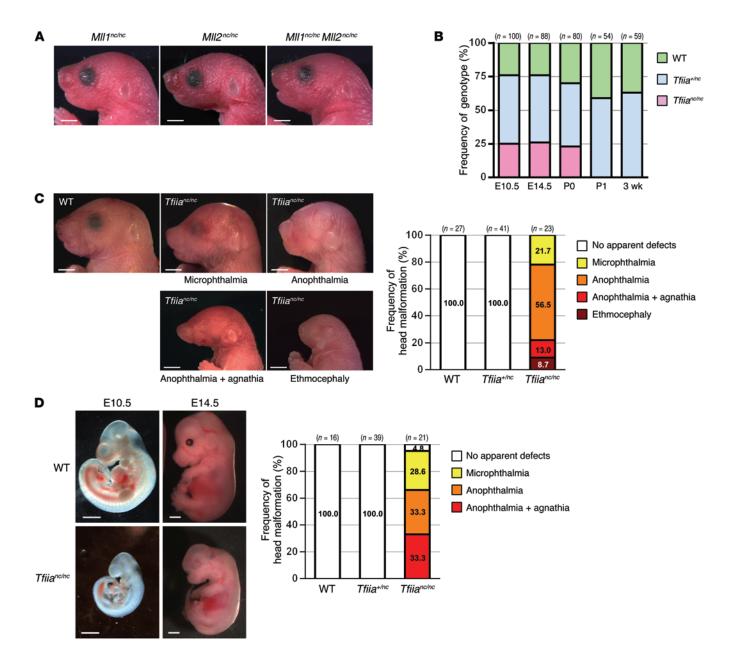
Figure 5. Genetic knockin of cleavage-resistant forms of TASP1 substrates reveals that noncleavage of TFIIAα-β phenocopies the craniofacial malformations observed in *Tasp1⁻/⁻* mice. (**A**) *Mll1^nc/nc^*, *Mll2^nc/nc^*, and *Mll1^nc/nc^ Mll2^nc/nc^* mice at P0 did not display craniofacial defects. Scale bar: 2.0 mm. (**B**) WT, *Tfiia^+/nc^*, and *Tfiia^nc/nc^* mice obtained from *Tfiia^+/nc^* intercrosses were observed at the expected Mendelian ratios at the indicated developmental stages. Nearly 100% of *Tfiia^nc/nc^* mice died within the first day of birth. (**C**) *Tfiia^nc/nc^* P0 animals exhibited head malformations similar to those observed in *Tasp1⁻/⁻* animals. Scale bar: 2.0 mm. (**D**) WT and *Tfiia^nc/nc^* E10.5 and E14.5 embryos with head malformations. Frequencies of the otocephalic phenotypes in E14.5 WT, *Tfiia^+/nc^*, and *Tfiia^nc/nc^* embryos are shown. Scale bar: 1.0 mm.

p16Ink4a, *p19Arf*, and *p21Cip1* were 2- to 3-fold higher in *Tasp1⁻/⁻* heads than in WT E10.5 heads (Figure 4C). Expression of *Ccne1* and *Ccna2*, which were previously identified as TASP1-regulated genes in MEFs (19), was only minimally reduced *Tasp1⁻/⁻* heads (Figure 4C).

We further determined the mRNAs levels of head organizer genes, including *Otx2*, *Hex*, *Hesx1*, and *Dkk1*, and did not detect significantly altered expression in *Tasp1⁻/⁻* E9.5 embryos (Supplemental Figure 2B). Of note, *Hex* expression was reduced by 25% (Supplemental Figure 2B). Since heterozygous loss of *Hex* does not induce overt craniofacial aberration (6), the observed *Hex*

reduction is unlikely to account for the drastic malformations of the *Tasp1⁻/⁻* embryo heads. Since MLL1, a substrate of TASP1, was shown to activate expression of MMP1 and MMP3 via interaction with ETS2 transcription factor (40) and remodeling of extracellular matrix is important for tissue morphogenesis, we determined the expression of several MMPs (Supplemental Figure 2C). In *Tasp1⁻/⁻* E10.5 embryos, *Mmp3* was reduced. Of note, mice deficient in *Mmp3* did not exhibit any craniofacial defects (41). Hence, the *Mmp3* reduction is unlikely to account for the overt head defects of *Tasp1⁻/⁻* animals. There were no significant differences in the expression of *Mt1-Mmp*, which is required for cranial skeleton
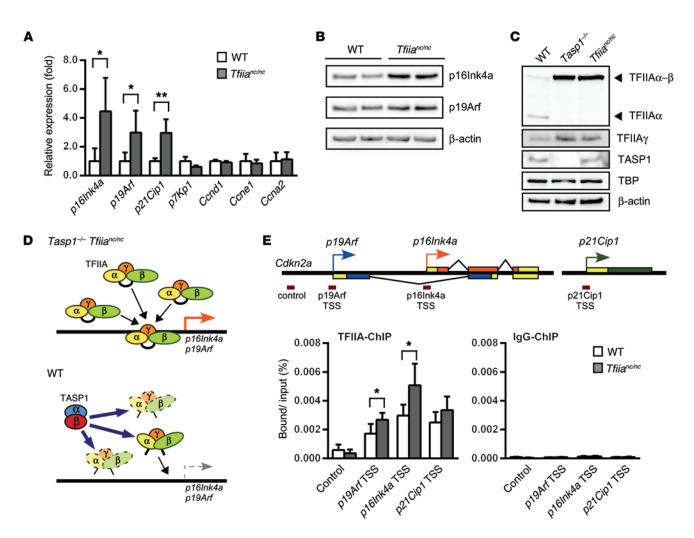
Figure 6. Loss of TFIIAα-β proteolysis leads to TFIIA stabilization at the *Cdkn2a* locus. (**A**) Quantitative RT-PCR detected increased *p16Ink4a*, *p19Arf*, and *p21Cip1* mRNA levels in *Tfiia^nc/nc* E10.5 embryo heads relative to levels in WT embryo heads. The mean was calculated from *n* = 3 (*Tfiia^nc/nc*) and *n* = 5 (WT). Error bars represent SD. *$P < 0.05$, **$P < 0.01$, unpaired 2-tailed Student's *t* test. (**B**) Immunoblots of WT and *Tfiia^nc/nc* MEFs validated increased levels of p16Ink4a and p19Arf proteins in *Tfiia^nc/nc* cells. (**C**) Immunoblots showing levels of TFIIAα, TFIIAα-β, TFIIAγ, TASP1, TBP, and β-actin in WT, *Tasp1^-/-*, and *Tfiia^nc/nc* E10.5 embryo heads. Note the accumulation of TFIIAα-β in the *Tasp1^-/-* and *Tfiia^nc/nc* lysates. (**D**) Illustration depicting the role of TFIIA in *p16Ink4a* and *p19Arf* regulation. During craniofacial development, TASP1-mediated cleavage of TFIIAα-β promotes TFIIA degradation, resulting in limited *p16Ink4a* and *p19Arf* transcription. (**E**) ChIP assay detected an increase of TFIIA at the *Cdkn2a* locus of *Tfiia^nc/nc* E10.5 embryo heads relative to that in WT embryo heads. TFIIA binding relative to input was quantified as a percentage by quantitative RT-PCR targeting the *p16Ink4a* transcription start site (TSS), the *p19Arf* transcription start site, and the *Cdkn2a* 3-kb upstream sequence (control) (*n* = 4 [*Tfiia^nc/nc*]; *n* = 5 [WT]). Error bars represent SD. *$P < 0.05$, unpaired 2-tailed Student's *t* test.

development, between WT and *Tasp1^-/-* embryos (Supplemental Figure 2C) (42). Furthermore, *Tasp1^-/-* embryos did not exhibit significant alteration in the expression of *Sox1* and *Sox2*, two key regulators of neuroectoderm (43). Overall, these results suggest that TASP1 is necessary for expansion of the prosencephalon, in part through its restriction of *p16Ink4a*, *p19Arf*, and *p21Cip1* expression.

To test the hypothesis that cell cycle regulation constitutes the key mechanism by which TASP1 coordinates mammalian cranial morphogenesis, we generated mice deficient in both *Tasp1* and *Cdkn2a*, using *Cdkn2a^-/-* mice, in which both *p16Ink4a* and *p19Arf* are deficient, on a pure C57BL/6 background. Remarkably, the deletion of *Cdkn2a* in our *Tasp1^-/- Cdkn2a^-/-* mice significantly rescued the head and body size anomalies of *Tasp1^-/-* mice (Figure 4, C and D). A greater proportion of E14.5 *Tasp1^-/- Cdkn2a^-/-* embryos developed a normal head (35.9% in *Tasp1^-/- Cdkn2a^-/-* embryos

versus 5.7% in *Tasp1^-/-* embryos), and a smaller proportion failed to develop a prosencephalon (5.1% in *Tasp1^-/- Cdkn2a^-/-* embryos versus 18.3% in *Tasp1^-/-* embryos) (Figure 4D). To further understand how p16Ink4a and p19Arf contribute to craniofacial development, we generated *Tasp1^-/- p16Ink4a^-/-* and *Tasp1^-/- p19Arf^-/-* mice, respectively, using *p16Ink4a^-/-* and *p19Arf^-/-* mice on a C57BL/6 background. Deficiency of *p16Ink4a* reduced the incidence of prosencephalon loss (9.7% in *Tasp1^-/- p16Ink4a^-/-* embryos versus 18.3% in *Tasp1^-/-* embryos) (Figure 4D). However, neither *p16Ink4a* nor *p19Arf* deficiency alone rescued the gross craniofacial defects of *Tasp1^-/-* mice. Thus, it is likely that suppression of both *p16Ink4a* and *p19Arf* during cranial morphogenesis is crucial for normal head development.

Tfiia^nc/nc *mice exhibit the same craniofacial malformations as* *Tasp1^-/-* *mice.* In mammals, the bona fide substrates proteolyzed

by TASP1 are TFIIAα-β, ALFα-β, MLL1, and MLL2. ALFα-β is expressed predominantly in the testes and ovaries (44–46), whereas TFIIAα-β, MLL1, and MLL2 are expressed ubiquitously, including in the head. Hence, we investigated whether TASP1-mediated cleavage of MLL1, MLL2, or TFIIAα-β contributes to head morphogenesis. $Mll1^{nc/nc}$, $Mll2^{nc/nc}$, and $Mll1^{nc/nc}$ $Mll2^{nc/nc}$ knockin mice carry homozygous noncleavable mutant $Mll1$ and/or $Mll2$ alleles at their native genomic loci (19, 32). None of these mice displayed craniofacial defects on a C57BL/6 background (N10) (Figure 5A). This result is consistent with our previous findings in MEFs that TASP1-mediated cleavage of MLLs regulates cyclin genes but not CDKIs (19). Hence, we generated homozygous $Tfiia^{nc/nc}$ mice (32) that were backcrossed with C57BL/6 mice. Like $Tasp1^{-/-}$ pups, $Tfiia^{nc/nc}$ pups on the C57BL/6 background–enriched background (N6) were born at the expected Mendelian ratio from $Tfiia^{+/nc}$ (N6) intercrosses and succumbed to death within the first day after birth (Figure 5B). Remarkably, $Tfiia^{nc/nc}$ and $Tasp1^{-/-}$ mice displayed closely similar otocephalic phenotypes and diminished body sizes at birth (Figure 5C) and during embryogenesis (Figure 5D). Of note, $Tfiia$ is expressed ubiquitously in E10.5 embryos (Supplemental Figure 3A), and thereby, the expression of $Tasp1$ likely dictates where cleaved TFIIA functions. Notably, none of the $Tfiia^{nc/nc}$ mice exhibited acephaly (P0) or prosencephalon loss (E14.5). This result suggests that proteolysis of TFIIAα-β may not be the only way that TASP1 regulates craniofacial development. Therefore, we generated triple mutant $Tfiia^{nc/nc}$ $Mll1^{nc/nc}$ $Mll2^{nc/nc}$ animals. However, introduction of $Mll1^{nc}$ and $Mll2^{nc}$ alleles into $Tfiia^{nc/nc}$ mice did not increase the severity of cranial anomalies (Supplemental Figure 3B).

Noncleaved TFIIAα-β is stabilized and targets to the Cdkn2a locus. Thus far, our genetic results demonstrate that (a) $Tasp1^{-/-}$ mice exhibited severe cranial anomalies with disrupted cell proliferation, (b) homozygous loss of $Cdkn2a$ significantly rescued these defects, and (c) $Tasp1^{-/-}$ mice and $Tfiia^{nc/nc}$ mice displayed a highly similar spectrum of cranial anomalies. Based on these findings, we hypothesized that TASP1 may promote proper head morphogenesis through the cleavage of TFIIAα-β to prevent undesirable aberrant transcription of $p16Ink4a$ and $p19Arf$. Accordingly, we investigated whether loss of TASP1-mediated cleavage of TFIIAα-β alters the expression of major cell cycle regulators in $Tfiia^{nc/nc}$ heads. Quantitative RT-PCR and immunoblotting revealed upregulation of $p16Ink4a$, $p19Arf$, and $p21Cip1$ but no changes in the mRNA levels of of $Ccnd1$, $Ccne1$, and $Ccna2$ (Figure 6, A and B), supporting TASP1/TFIIA regulation of p16Ink4a/p19Arf/p21Cip1 as an important regulatory axis in cranial morphogenesis.

Next, we examined how TASP1-mediated cleavage of TFIIAα-β prevents induction of $p16Ink4a$ and $p19Arf$. Previous studies have shown that noncleaved TFIIAα-β is less susceptible to proteasome-mediated degradation than its cleaved form (31). Consistently, immunoblotting of TFIIA protein in E10.5 $Tasp1^{-/-}$ and $Tfiia^{nc/nc}$ heads showed an accumulation of noncleaved TFIIAα-β (Figure 6C). Interestingly, the TFIIAγ subunit of TFIIA also exhibited stabilization in $Tasp1^{-/-}$ and $Tfiia^{nc/nc}$ lysates, albeit to a lesser extent than TFIIAα-β (Figure 6C). Notably, TFIIAγ exhibited stabilization in $Tasp1^{-/-}$ and $Tfiia^{nc/nc}$ lysates, but not in $Tfiia^{+/nc}$ lysate (Supplemental Figure 3C), suggesting that TFIIAγ is stabilized only when all of the TFIIAα-β stays noncleaved. These results suggest that

TASP1-mediated cleavage of TFIIAα-β contributes to the steady-state transcription by regulating TFIIA turnover. Noncleaved TFIIAα-β retains its cleaved form's ability to bind TBP and is transcriptionally active (30). Accretion of high levels of noncleaved TFIIAα-β through either cleavage site mutation ($Tfiia^{nc/nc}$) or loss of TASP1 function ($Tasp1^{-/-}$) should therefore increase the association of TFIIA at the TFIIA target gene loci (Figure 6D). We tested this hypothesis by performing ChIP assays on the heads of E10.5 $Tfiia^{nc/nc}$ and WT embryos. Indeed, we observed a significant increase in TFIIA occupancy at $p16Ink4a$ and $p19Arf$ promoters in $Tfiia^{nc/nc}$ embryos (Figure 6E).

Discussion

The morphogenesis of the vertebrate head, which is composed of a group of the most elaborate organs in the body, demands a series of dynamic events, coordinating the proliferation, migration, and patterning of different lineages of cells. Brain vesicles, the prosencephalon, mesencephalon, and rhombencephalon, derive from the anterior neuroectoderm (9). Defects in induction of the anterior neuroectoderm in mouse models deficient in $Otx2$, $Lim1$, $Ssdp1$, and Hex commonly result in the absence of the prosencephalon by E8.5 and acephaly at P0, if not in prenatal lethality (3–5). In this study, we identified a variety of craniofacial defects in $Tasp1^{-/-}$ pups at P0 (Figure 1B). However, $Tasp1^{-/-}$ embryos at E8.5 displayed no overt defects in the prosencephalon (Figure 2A), and acephaly was an uncommon phenotype of P0 $Tasp1^{-/-}$ pups (Figure 1C). These observations indicate that TASP1 plays a role in the events subsequent to anterior neuroectoderm induction.

Importantly, the most common phenotype of $Tasp1^{-/-}$ embryos was hypoplasia of the prosencephalon starting at E9.5 (Figure 2, A and B). The prosencephalon serves as a signaling center and a structural support that is critical for the development of craniofacial tissues. For example, the optic vesicle, which develops in the lateral wall of the diencephalon, releases BMP4 and induces the lens placode (47, 48). Sonic hedgehog (Shh) expressed in the ventral prosencephalon is essential for expansion of the frontonasal process that develops into the nose and upper jaw (49, 50). Furthermore, expression of Shh in the anterior foregut endoderm immediately beneath the prosencephalon was shown to be pivotal for the induction of the first pharyngeal arch, which develops into lower jaw (51, 52). Consistently, frequency analysis of the craniofacial defects of $Tasp1^{-/-}$ animals suggested that the shrunken prosencephalon in E10.5 embryos results in anophthalmia or microphthalmia at E14.5 and P0, while prosencephalon loss at E10.5 results in agnathia in addition to eye defects (Figure 1C and Supplemental Figure 2A), suggesting development of eyes is dependent on intact prosencephalon. Histologically, the hypoplastic prosencephalons of E10.5 $Tasp1^{-/-}$ embryos displayed reduced thickness of the telencephalic neuroectoderm, overall impaired cell proliferation, and restriction of a few proliferating cells to the ventricular side (Figure 3A). The telencephalic neuroectoderm of E10.5 WT embryos consisted primarily of the ventricular zone (VZ) on the lumenal side and the subventricular zone (SVZ) on the surface side. In the VZ, apical neural progenitor cells undergo asymmetric divisions to produce intermediate neural progenitor cells and neurons. Intermediate neural progenitor cells translocate externally to form the SVZ, in which they undergo symmetric divisions (53). The histological features of

Tasp1⁻/⁻ embryos suggest that TASP1 may be required primarily for the division of intermediate neural progenitors in the SVZ and thus for expansion of the SVZ.

Of all the cranial organs, the brain experiences the most dramatic expansion during inflation of the brain vesicles. Cell proliferation is locally regulated to shape the complex structure of the brain. For instance, the cells in the alar region of the neural plate proliferate more than those in the floor region to enable neural tube closure (13). The cells in the prosencephalic vesicle proliferate more than the cells at the boundary between the prosencephalon and the mesencephalon to enable prosencephalon expansion (12). However, the molecular machinery regulating cell proliferation in early brain development is poorly understood. Several cell cycle regulators, including cyclin D2, p21Cip1, p27Kip1, and p57Kip2, have been implicated in corticogenesis but not in early craniofacial development (54–56). None of the mouse models with cyclin, CDK, or CDKI deficiency exhibit critical craniofacial defects other than changes in the thickness of limited cerebral cortical layers (14, 15), most likely because of functional redundancy among cell cycle regulators. The relevance of negative cell cycle regulators p16Ink4a and p19Arf to embryonic development has long been dismissed, as their expression is barely detectable in mouse embryos (E7.5–E17.5) by Northern blot (57). However, *p16Ink4a* and *p19Arf* levels increase over passages of MEFs, suggesting that *p16Ink4a* and *p19Arf* transcription is actively repressed during embryogenesis (57). Here, we discovered that TASP1 depletion leads to robust upregulation of *p16Ink4a* and *p19Arf* in developing mouse heads (Figure 4C). We showed that compound deficiency of *Cdkn2a*, the locus from which *p16Ink4a* and *p19Arf* are transcribed, significantly rescues the craniofacial anomalies of *Tasp1⁻/⁻* animals, thereby demonstrating that p16Ink4a and p19Arf play an important role in craniofacial development (Figure 4C). *Cdkn2a* deficiency rescued all of the observed craniofacial phenotypes of *Tasp1⁻/⁻* embryos, including anophthalmia and agnathia, indicating that cell cycle deregulation is the principal defect that TASP1 depletion causes. However, *Cdkn2a* deficiency did not affect a complete rescue: more than 60% of *Tasp1⁻/⁻ Cdkn2a⁻/⁻* animals still showed craniofacial defects (Figure 4C). One hypothesis that accounts for this incomplete rescue is that p21Cip1, another CDKI that showed upregulation in *Tasp1⁻/⁻* embryos, also contributes to craniofacial defects and that p21Cip1 and p16Ink4a have redundant roles in cell cycle regulation. This hypothesis could be tested by examining the rescue of *Tasp1⁻/⁻* phenotypes by deficiencies of both *Cdkn2a* and *p21Cip1*. An alternative hypothesis is that cell cycle regulation is not the only mechanism by which TASP1 coordinates craniofacial morphogenesis. This latter hypothesis is supported by our characterization of *Tfiia^nc/nc^* embryos, none of which exhibited prosencephalon loss at E14.5 or acephaly at P0 (Figure 5, B–D), despite displaying clear upregulation of *p16Ink4a*, *p19Arf*, and *p21Cip1* (Figure 6A).

In a previous study on MEFs, we demonstrated that TASP1 loss leads to concurrent downregulation of *Ccne1*, *Ccna2*, and *Ccnb* and upregulation of CDKIs *p16*, *p21*, and *p27* (19). We also provided evidence that TASP1 helps MLL1 and MLL2 regulate the expression of cyclin genes by activating their histone methyltransferase activities (ref. 19 and Supplemental Figure 4). Interestingly, we did not observe significant downregulation of cyclin genes in

the *Tasp1⁻/⁻* embryo heads, possibly reflecting the tissue specificity. In addition to cyclin genes, MLL1 and MLL2 also drive transcription of *Hox* genes, which regulate specification of the anterior-posterior axis during embryogenesis (38). However, *Hox* genes seem irrelevant to the craniofacial anomalies caused by TASP1 deficiency, because no *Hox* genes are expressed anterior to the rhombencephalon, and none of the *Hox*-deficient mouse models reportedly display craniofacial phenotypes observed in *Tasp1⁻/⁻* embryos (Mouse Genome Informatics, http://www.informatics.jax.org). Consistently, *Mll1^nc/nc^*, *Mll2^nc/nc^*, and *Mll1^nc/nc^ Mll2^nc/nc^* mice displayed no obvious craniofacial defects, thus we concluded that TASP1-mediated proteolysis of MLL1 and MLL2 is dispensable for normal head development.

In contrast to cyclin genes, how TASP1 controls the transcription of CDKIs has been an open question. Here, we discovered that failure in TASP1-mediated proteolysis of TFIIAα-β in *Tfiia^nc/nc^* animals resulted in a robust increase of *p16Ink4a* and *p19Arf* (Figure 6, A and B), thus demonstrated a signaling cascade that we believe to be novel comprising TASP1 (protease), TFIIA (general transcription factor), and CDKN2A (cell cycle regulators). We displayed in mouse embryos that noncleavage of TFIIAα-β leads to increased protein stability of TFIIAα-β and TFIIAγ, consistent with the previous finding in vitro that TASP1-mediated proteolysis of TFIIAα-β accelerates proteasome-mediated degradation (31). Noncleaved TFIIAα-β was shown to interact with TBP and TFIIAγ and enhance transcription as efficiently as its cleaved form (31, 58). Consequently, our findings in vivo suggest that the primary function of TASP1-mediated TFIIA proteolysis is the regulation of cellular levels of TFIIA. Our ChIP assays showed that stabilization of TFIIAα-β in *Tfiia^nc/nc^* embryos leads to significantly increased TFIIA occupancy on *p16Ink4a* and *p19Arf* promoters. Accordingly, we concluded that TASP1 cleaves TFIIAα-β to prevent excess recruitment of TFIIAα-β to *p16Ink4a* and *p19Arf* promoters during mammalian cranial morphogenesis. Recently, we elucidated a specific role for TASP1-mediated proteolysis of TFIIAα-β in mammalian spermatogenesis (32). Proteolysis activated TFIIA's ability to recruit TRF2 for the upregulation of spermiogenic genes (*Tnp* and *Prm*) through targeting respective promoters (Supplemental Figure 4), and *Tfiia^nc/nc^* animals display immature spermiogenesis in spite of the improved protein stability that noncleavage confers on TFIIAα-β (32). Notably, it is unlikely that recruitment of TRF2 by proteolyzed TFIIAα-β occurs during craniofacial morphogenesis, because the phenotype of TRF2-deficient mice is limited to defects in spermiogenesis. Animals deficient in TRF2 incur neither other embryogenesis defects nor lethality (59). Hence, TASP1 uses various strategies to achieve sophisticated control over diverse biological processes.

Methods

ations (N10). Skeletal studies were performed as previously described (19). Briefly, skulls were stained with alizarin red and alcian blue for visualization of bone and cartilage, respectively. Mouse embryos and P0 pups were photographed with an Infinity camera (Lumenera) under a stereoscopic microscope (Zeiss Stemi 2000-C, Zeiss). For measurement of embryo body sizes, a digital image of each embryo was converted into a binary file. The distance between the ears and the tail base was then calculated using the Measure Roi Curve plug-in for the ImageJ software program.

MEFs. MEFs were harvested from WT and *Tfiia^{nc/nc}* E13.5 mouse embryos according to the standard protocol (60). MEFs were cultured in Iscove's Modified Dulbecco's Medium supplemented with 20% fetal bovine serum.

Histology, immunohistochemistry, and cell quantification. Tissues or whole embryos were collected and fixed in 4% paraformaldehyde (PFA) or Bouin's solution. Paraffin-embedded samples were sectioned (5–7 μm), rehydrated, and subjected to hematoxylin and eosin staining, immunohistochemistry (IHC), or Hoechst (Invitrogen) staining. For IHC of sections, samples were blotted with the antibody specific to pHH3 Ser10 (06-570, Upstate) or cleaved Caspase-3 (9661, Cell Signaling) and visualized with DAB and nickel chloride (Vector Labs). For whole-mount IHC, E10.5 embryos were bleached in 6% H_2O_2/methanol and dehydrated in 100% methanol. Samples were blocked in 5% skim milk and 1% Triton X-100 in PBS and incubated with anti-CD31 antibody (557355, BD Pharmingen). Following incubation with peroxidase-conjugated anti-rat IgG, staining was visualized with the DAB Peroxidase Substrate Kit (Vector Labs). Images were acquired with a SPOT camera (Diagnostics Instruments) mounted on an Olympus IX51 microscope (Olympus). Where indicated, cell numbers were determined using the ITCN plug-in for the ImageJ software program and normalized to the number of Hoechst-positive cells.

In situ hybridization. Whole-mount in situ hybridization was performed on E10.5 mouse embryos. The cDNAs of mouse *Tasp1* and *Tfiia1* were used as the templates to generate RNA probes. Embryos were fixed with 4% PFA in PBS, permeabilized with proteinase K, and then post-fixed with 4% PFA and 0.2% glutaraldehyde in PBS. Hybridization was performed overnight at 65°C with DIG-labeled RNA probes in hybridization buffer (50% formamide, 5x SSC, 0.3 mg/ml yeast RNA, 0.1 mg/ml heparin, 1x Denhardt's, 0.1% Tween 20, and 5 mM EDTA). Embryos were washed with 50% formamide in 2x SSC, blocked in 1.5% Blocking Reagent (Roche) in KTBT (50 mM Tris-HCl, 140 M NaCl, 10 mM KCl, 0.1% Tween 20), and incubated overnight at 4°C with AP-conjugated anti-DIG Fab fragments (Roche). After extensive washes, the color reaction was carried out using BM purple (Roche).

RNA isolation, quantitative RT-PCR, and microarray analysis. For RNA isolation, surgically dissected E10.5 mouse heads (prosencephalons and mesencephalons) were homogenized in TRIzol reagent (Invitrogen) using FastPrep-24 and Lysing Matrix D (MP Biomedicals). cDNA was produced from total RNA extracted using SuperScript II (Invitrogen), oligo-dT (Invitrogen), and random decamer primers (Ambion) according to the manufacturer's instructions. Quantitative RT-PCR was performed using SYBR Green Master Mix (Applied Biosystems), gene-specific oligonucleotide primers (listed in Supplemental Table 2), and the

ViiA7 Real-Time PCR System (Applied Biosystems). Gene expression data were normalized against *Gapdh* detected using a *Gapdh* TaqMan probe (Applied Biosystems). For microarray analysis, samples prepared from RNA isolated from E10.5 prosencephalons and mesencephalons were hybridized to GeneChip Mouse ST 1.0 (Affymetrix). The expression signals were subjected to Gene Ontology analysis (Partek) and GSEA (http://www.broadinstitute.org/gsea/index.jsp) to identify overrepresented groups of genes, with common biological processes or pathways. Microarray data were deposited in GEO (accession no. GSE64533).

Immunoblot analysis. Dissected E10.5 mouse heads (prosencephalons and mesencephalons) or E13.5 primary MEFs at passage P2 were lysed in RIPA buffer supplemented with complete protease inhibitors (Roche). The mouse head lysates were homogenized for complete dissociation using FastPrep-24 and Lysing Matrix D (MP Biomedicals). Samples were loaded onto NuPAGE gels (Invitrogen) and transferred onto PVDF (Immobilon-P, Millipore). Proteins of interest were blotted with specific antibodies and detected with enhanced chemiluminescence reagents (Western Lightening, Perkin Elmer) and the LAS-300 Imaging System (FUJIFILM Life Science). Antibodies against TASP1 and TFIIAα (SM346) are as previously described (32, 61); antibodies against p16Ink4a (sc74401, Santa Cruz), p19Arf (ab26696, Abcam), TFIIAγ (sc5316, Santa Cruz), TBP (sc204, Santa Cruz), and anti–β-actin (AC-15, Sigma-Aldrich) were purchased commercially. See complete unedited blots in the supplemental material.

ChIP assay. Tissue was collected from the prosencephalons, mesencephalons, upper jaws, and eyes (but not from the rhombencephalons and lower jaws) of E12.5 mouse embryos; minced with a razor blade; and fixed with 1% PFA. The approximately 10 mg chromatin obtained from 4×10^6 to 5×10^6 cells was sonicated using a Bioruptor (Diagenode) for 28 minutes to sheer the DNA into fragments of 100 to 400 base pairs. Immunoprecipitation was performed using antibodies against TFIIAα (MO431) or rabbit IgG (Sigma-Aldrich) and anti-rabbit IgG Dynabeads (Invitrogen). The anti-TFIIAα antibody was generated by immunizing rabbits against the peptide encompassing aa 1–276 of human TFIIAα-β. Precipitated DNA was assessed by quantitative RT-PCR using gene-specific oligonucleotide primers (listed in Supplemental Table 2). The immunoprecipitation efficiency was determined as the percentage relative to input.

Statistics. Results are presented as mean ± SD. Except where otherwise specified, statistical significance was determined by unpaired 2-tailed Student's *t* test. A *P* value of less than 0.05 was considered significant.

Study approval. All animal work was performed in accordance to a protocol approved by the Institutional Animal Care and Use Committee of Memorial Sloan-Kettering Cancer Center.

Acknowledgments

Address correspondence to: James J. Hsieh, Human Oncology and Pathogenesis Program, Memorial Sloan-Kettering Cancer Center, 1275 York Ave., New York, New York 10065, USA. Phone: 646.888.3263; E-mail: hsiehj@mskcc.org.

1. Copp AJ, Greene ND. Genetics and development of neural tube defects. *J Pathol*. 2010;220(2):217–230.
2. Trainor PA. Craniofacial birth defects: The role of neural crest cells in the etiology and pathogenesis of Treacher Collins syndrome and the potential for prevention. *Am J Med Genet A*. 2010;152A(12):2984–2994.
3. Rhinn M, Dierich A, Shawlot W, Behringer RR, Le Meur M, Ang SL. Sequential roles for Otx2 in

visceral endoderm and neuroectoderm for forebrain and midbrain induction and specification. *Development*. 1998;125(5):845–856.

4. Shawlot W, Wakamiya M, Kwan KM, Kania A, Jessell TM, Behringer RR. Lim1 is required in both primitive streak-derived tissues and visceral endoderm for head formation in the mouse. *Development*. 1999;126(22):4925–4932.

5. Nishioka N, et al. Ssdp1 regulates head morphogenesis of mouse embryos by activating the Lim-Ldb1 complex. *Development*. 2005;132(11):2535–2546.

6. Martinez Barbera JP, et al. The homeobox gene Hex is required in definitive endodermal tissues for normal forebrain, liver and thyroid formation. *Development*. 2000;127(11):2433–2445.

7. Dattani MT, et al. Mutations in the homeobox gene HESX1/Hesx1 associated with septo-optic dysplasia in human and mouse. *Nat Genet*. 1998;19(2):125–133.

8. Niehrs C. Head in the WNT: the molecular nature of Spemann's head organizer. *Trends Genet*. 1999;15(8):314–319.

9. Perea-Gomez A, Rhinn M, Ang SL. Role of the anterior visceral endoderm in restricting posterior signals in the mouse embryo. *Int J Dev Biol*. 2001;45(1):311–320.

10. Desmond ME, O'Rahilly R. The growth of the human brain during the embryonic period proper. 1. Linear axes. *Anat Embryol (Berl)*. 1981;162(2):137–151.

11. Tuckett F, Morriss-Kay GM. The kinetic behaviour of the cranial neural epithelium during neurulation in the rat. *J Embryol Exp Morphol*. 1985;85:111–119.

12. Kahane N, Kalcheim C. Identification of early postmitotic cells in distinct embryonic sites and their possible roles in morphogenesis. *Cell Tissue Res*. 1998;294(2):297–307.

13. Pombero A, Martinez S. Telencephalic morphogenesis during the process of neurulation: an experimental study using quail-chick chimeras. *J Comp Neurol*. 2009;512(6):784–797.

14. Gopinathan L, Ratnacaram CK, Kaldis P. Established and novel Cdk/cyclin complexes regulating the cell cycle and development. *Results Probl Cell Differ*. 2011;53:365–389.

15. Tury A, Mairet-Coello G, DiCicco-Bloom E. The multiple roles of the cyclin-dependent kinase inhibitory protein p57(KIP2) in cerebral cortical neurogenesis. *Dev Neurobiol*. 2012;72(6):821–842.

16. Hsieh JJ, Henkel T, Salmon P, Robey E, Peterson MG, Hayward SD. Truncated mammalian Notch1 activates CBF1/RBPJk-repressed genes by a mechanism resembling that of Epstein-Barr virus EBNA2. *Mol Cell Biol*. 1996;16(3):952–959.

17. Hsieh JJ, Cheng EH, Korsmeyer SJ. Taspase1: a threonine aspartase required for cleavage of MLL and proper HOX gene expression. *Cell*. 2003;115(3):293–303.

18. Khan JA, Dunn BM, Tong L. Crystal structure of human Taspase1, a crucial protease regulating the function of MLL. *Structure*. 2005;13(10):1443–1452.

19. Takeda S, et al. Proteolysis of MLL family proteins is essential for taspase1-orchestrated cell cycle progression. *Genes Dev*. 2006;20(17):2397–2409.

20. Zhou H, et al. Uncleaved TFIIA is a substrate for taspase 1 and active in transcription. *Mol Cell Biol*. 2006;26(7):2728–2735.

21. Capotosti F, Hsieh JJ, Herr W. Species selectivity of mixed-lineage leukemia/trithorax and HCF proteolytic maturation pathways. *Mol Cell Biol*. 2007;27(20):7063–7072.

22. Chen DY, et al. A pharmacologic inhibitor of the protease Taspase1 effectively inhibits breast and brain tumor growth. *Cancer Res*. 2012;72(3):736–746.

23. Dong Y, Van Tine BA, Oyama T, Wang PI, Cheng EH, Hsieh JJ. Taspase1 cleaves MLL1 to activate cyclin E for HER2/neu breast tumorigenesis. *Cell Res*. 2014;24(11):1354–1366.

24. Roeder RG. Role of general and gene-specific cofactors in the regulation of eukaryotic transcription. *Cold Spring Harb Symp Quant Biol*. 1998;63:201–218.

25. Veenstra GJ, Wolffe AP. Gene-selective developmental roles of general transcription factors. *Trends Biochem Sci*. 2001;26(11):665–671.

26. Kadonaga JT. Perspectives on the RNA polymerase II core promoter. *Wiley Interdiscip Rev Dev Biol*. 2012;1(1):40–51.

27. Buratowski S, Hahn S, Guarente L, Sharp PA. Five intermediate complexes in transcription initiation by RNA polymerase II. *Cell*. 1989;56(4):549–561.

28. Inostroza JA, Mermelstein FH, Ha I, Lane WS, Reinberg D. Dr1, a TATA-binding protein-associated phosphoprotein and inhibitor of class II gene transcription. *Cell*. 1992;70(3):477–489.

29. Kokubo T, Swanson MJ, Nishikawa JI, Hinnebusch AG, Nakatani Y. The yeast TAF145 inhibitory domain and TFIIA competitively bind to TATA-binding protein. *Mol Cell Biol*. 1998;18(2):1003–1012.

30. Mitsiou DJ, Stunnenberg HG. TAC, a TBP-sans-TAFs complex containing the unprocessed TFIIAalphabeta precursor and the TFIIAgamma subunit. *Mol Cell*. 2000;6(3):527–537.

31. Hoiby T, Mitsiou DJ, Zhou H, Erdjument-Bromage H, Tempst P, Stunnenberg HG. Cleavage and proteasome-mediated degradation of the basal transcription factor TFIIA. *EMBO J*. 2004;23(15):3083–3091.

32. Oyama T, et al. Cleavage of TFIIA by Taspase1 activates TRF2-specified mammalian male germ cell programs. *Dev Cell*. 2013;27(2):188–200.

33. Matsuo I, Kuratani S, Kimura C, Takeda N, Aizawa S. Mouse Otx2 functions in the formation and patterning of rostral head. *Genes Dev*. 1995;9(21):2646–2658.

34. Shawlot W, Behringer RR. Requirement for Lim1 in head-organizer function. *Nature*. 1995;374(6521):425–430.

35. Acampora D, et al. Forebrain and midbrain regions are deleted in Otx2−/− mutants due to a defective anterior neuroectoderm specification during gastrulation. *Development*. 1995;121(10):3279–3290.

36. Mukhopadhyay M, et al. Functional ablation of the mouse Ldb1 gene results in severe patterning defects during gastrulation. *Development*. 2003;130(3):495–505.

37. Mukhopadhyay M, et al. Dickkopf1 is required for embryonic head induction and limb morphogenesis in the mouse. *Dev Cell*. 2001;1(3):423–434.

38. Alexander T, Nolte C, Krumlauf R. Hox genes and segmentation of the hindbrain and axial skeleton.

Annu Rev Cell Dev Biol. 2009;25:431–456.

39. Sherr CJ. The INK4a/ARF network in tumour suppression. *Nat Rev Mol Cell Biol*. 2001;2(10):731–737.

40. Takeda S, et al. HGF-MET signals via the MLL-ETS2 complex in hepatocellular carcinoma. *J Clin Invest*. 2013;123(7):3154–3165.

41. Mudgett JS, et al. Susceptibility of stromelysin 1-deficient mice to collagen-induced arthritis and cartilage destruction. *Arthritis Rheum*. 1998;41(1):110–121.

42. Holmbeck K, et al. MT1-MMP-deficient mice develop dwarfism, osteopenia, arthritis, and connective tissue disease due to inadequate collagen turnover. *Cell*. 1999;99(1):81–92.

43. Marques-Torrejon MA, et al. Cyclin-dependent kinase inhibitor p21 controls adult neural stem cell expansion by regulating Sox2 gene expression. *Cell Stem Cell*. 2013;12(1):88–100.

44. Yu BD, Hess JL, Horning SE, Brown GA, Korsmeyer SJ. Altered Hox expression and segmental identity in Mll-mutant mice. *Nature*. 1995;378(6556):505–508.

45. Glaser S, et al. Multiple epigenetic maintenance factors implicated by the loss of Mll2 in mouse development. *Development*. 2006;133(8):1423–1432.

46. Xiao L, Kim M, DeJong J. Developmental and cell type-specific regulation of core promoter transcription factors in germ cells of frogs and mice. *Gene Expr Patterns*. 2006;6(4):409–419.

47. Furuta Y, Hogan BL. BMP4 is essential for lens induction in the mouse embryo. *Genes Dev*. 1998;12(23):3764–3775.

48. Sjodal M, Edlund T, Gunhaga L. Time of exposure to BMP signals plays a key role in the specification of the olfactory and lens placodes ex vivo. *Dev Cell*. 2007;13(1):141–149.

49. Marcucio RS, Cordero DR, Hu D, Helms JA. Molecular interactions coordinating the development of the forebrain and face. *Dev Biol*. 2005;284(1):48–61.

50. Hu D, Marcucio RS. A SHH-responsive signaling center in the forebrain regulates craniofacial morphogenesis via the facial ectoderm. *Development*. 2009;136(1):107–116.

51. Le Douarin NM, Brito JM, Creuzet S. Role of the neural crest in face and brain development. *Brain Res Rev*. 2007;55(2):237–247.

52. Dennis JF, et al. Mutations in Hedgehog acyltransferase (Hhat) perturb Hedgehog signaling, resulting in severe acrania-holoprosencephaly-agnathia craniofacial defects. *PLoS Genet*. 2012;8(10):e1002927.

53. Farkas LM, Huttner WB. The cell biology of neural stem and progenitor cells and its significance for their proliferation versus differentiation during mammalian brain development. *Curr Opin Cell Biol*. 2008;20(6):707–715.

54. Glickstein SB, Monaghan JA, Koeller HB, Jones TK, Ross ME. Cyclin D2 is critical for intermediate progenitor cell proliferation in the embryonic cortex. *J Neurosci*. 2009;29(30):9614–9624.

55. Mairet-Coello G, Tury A, Van Buskirk E, Robinson K, Genestine M, DiCicco-Bloom E. p57(KIP2) regulates radial glia and intermediate precursor cell cycle dynamics and lower layer neurogenesis in developing cerebral cortex. *Development*. 2012;139(3):475–487.

56. Siegenthaler JA, Miller MW. Transforming growth factor beta 1 promotes cell cycle exit through the cyclin-dependent kinase inhibitor p21 in the developing cerebral cortex. *J Neurosci*. 2005;25(38):8627–8636.

57. Zindy F, Quelle DE, Roussel MF, Sherr CJ. Expression of the p16INK4a tumor suppressor versus other INK4 family members during mouse development and aging. *Oncogene*.

1997;15(2):203–211.

58. Sun X, Ma D, Sheldon M, Yeung K, Reinberg D. Reconstitution of human TFIIA activity from recombinant polypeptides: a role in TFIID-mediated transcription. *Genes Dev*. 1994;8(19):2336–2348.

59. Zhang D, Penttila TL, Morris PL, Teichmann M, Roeder RG. Spermiogenesis deficiency in mice lacking the Trf2 gene. *Science*.

2001;292(5519):1153–1155.

60. Ren D, et al. BID, BIM, and PUMA are essential for activation of the BAX- and BAK-dependent cell death program. *Science*. 2010;330(6009):1390–1393.

61. Chen DY, et al. Taspase1 functions as a non-onco-gene addiction protease that coordinates cancer cell proliferation and apoptosis. *Cancer Res*. 2010;70(13):5358–5367.